



ENERGY DISSIPATION COMPONENTS OF PRECAST CONCRETE SINGLE ROCKING WALLS

M. Nazari⁽¹⁾, S. Sritharan⁽²⁾

⁽¹⁾ Graduate Research Assistant, Iowa State University, Ames, Iowa, US, mnazari@iastate.edu

⁽²⁾ Wilson Engineering Professor, Iowa State University, Ames, Iowa, US, sri@iastate.edu

Abstract

Though not widely used in practice due to their limited energy dissipation capacity, recent research has shown that single post-tensioned precast concrete rocking walls can be used to satisfactorily resist earthquake loads. These walls, dissipate energy imparted to them during rocking due to the wall impacting the foundation, limited hysteretic action resulting from concrete nonlinearity, and inherent viscous damping. Relying only on the limited energy dissipation, a shake table study was conducted on four Single Rocking Walls (SRWs) using multiple-level earthquake input motions. Using the experimental data, participation of different damping components of SRWs in their seismic energy dissipation was evaluated. On average, an equivalent viscous damping ratio of 6% was estimated for SRWs, with dynamic impacts contributing to about one third of the total damping. For analytical predictions, it is shown that the impact energy loss can be satisfactorily captured using a 3% tangent stiffness damping. Despite the low amount of energy dissipation, all four SRWs generally produced satisfactory responses. While the peak displacement was somewhat higher due to the low amount of energy dissipation, the duration of rocking of these walls was found to be reduced by negative rate of input energy, which ultimately reduced the seismic energy imparted to the walls.

Keywords: unbonded Post-tensioning, precast concrete, rocking walls, energy dissipation, shake table testing



1. Introduction

Precast concrete walls with post-tensioning (PT) as a possible lateral load-resisting system have been studied for nearly two decades [e.g., 1]. Unbonded PT is used as the primary reinforcement in these walls to enable them to resist lateral forces. In addition, the tendons are designed to remain elastic when subjected to design-level earthquakes, thereby enabling the walls to self center when the lateral load is removed. As a result, these Single Rocking Walls (SRWs) are expected to exhibit a bilinear elastic behavior with minimal hysteretic energy dissipation capacity. SRWs also dissipate a part of seismic input energy through impacts when the wall uplifts and impacts on top of the foundation. Due to their low energy dissipation capacities, use of SRWs is limited in seismic regions; instead, precast concrete walls incorporated with additional hysteretic dampers have been promoted for seismic design [2-4].

Two recent shake table studies conducted on SRWs indicated that they can produce satisfactory seismic performance when subjected to design-level and greater intensity earthquake ground motions [5, 6]. Marriot et al. [5] reported a shake table study on five post-tensioned walls, which included one SRW. When subjected to a near-field and a far-field design-level and maximum considered input motions, this SRW produced satisfactory response with the maximum drift staying below the target drift ratio of 1.5%. Using a free vibration test, the SRW was estimated to have an equivalent viscous damping ratio of 1 to 3%. Twigden [6] completed a series of shake table tests on two SRWs, which experienced a maximum lateral drift of 3.48%. The results from the snap back testing on these SRWs confirmed equivalent damping values between 0.9 and 3.8% for these walls, which included the damping due to impact.

This paper quantifies the different damping components that contribute to the energy dissipation of SRWs using shake table test data. The experimental results were also used to quantify the equivalent viscous damping ratio of SRWs to be considered for their seismic design and response evaluation. The corresponding damping ratio includes the following individual energy dissipation components: (1) the hysteretic energy dissipation due to concrete nonlinearity; (2) inherent viscous damping; and (3) energy loss due to impacts of the wall on top of the foundation. The estimated damping was then applied in a simplified analytical model to show that the measured shake table responses can be adequately reproduced. In addition to damping, it is also shown that during rocking response of SRWs, noticeable negative input energy rate may present, which helps to reduce the duration of wall response especially after it experienced peak lateral drifts.

2. Summary of Experimental Investigations

Four SRWs were tested at the NEES shake table facility of the University of Nevada at Reno (UNR). They were 190.5 cm (6.25 ft) long, 487.7 cm (16 ft) tall and 12.7 cm (5 in) thick, representing a prototype rocking wall in a six-story office building at a 5/18 scale. The prototype building was designed for a high seismic location in Los Angeles, California. These test walls were subjected to a series of scaled ground motions representing four seismic hazard levels, i.e., EQ-I to EQ-IV. As presented by SEOAC seismology committee [7], these hazard levels are defined by five percent damped elastic acceleration response spectra. Hazard levels of EQ-III and EQ-IV, respectively, represent the design-based earthquake (DBE) and the maximum considered earthquake (MCE). The ground motions selected for this study are listed in Table 1. While the information provided in this table is at the prototype scale, the amplitude of all the motions was scaled up by 18/5 and the time step was decreased by a factor of 5/18 to satisfy the scale effects. The test matrix, as detailed in Table 2, includes the key design parameters such as the initial prestressing and area of PT tendons as well as their calculated lateral resistance at 2% drift as variables. A Simplified Analysis (SA) method presented by Aaleti and Sritharan [8] was used as a tool to design the amount of PT in SRWs. Observed seismic responses of the test walls in terms of lateral drift, absolute acceleration, and residual drift during DBE and MCE events are also summarized in this table. Accordingly, ratio of the maximum measured demands to the corresponding allowable limits were reported; these limits are defined based on the recommendations of Rahman and Sritharan [9] for different intensities of ground motions. Reported results show seismic performance of SRW3 and SRW4 designed with higher shear forces during design-level and larger earthquakes were satisfactory. More description about the prototype structure, design of the test walls, test set-up, and the loading protocol is presented in Nazari et al. [10].



Table 1 – List of ground motions

ID	Source	Earthquake Name (Year), Station, FF/NF	Scale factor	Targeted hazard level	PGA (g) after applying the scale factor
Eq-1s	Spectrum compatible short duration motions used in PRESSS building [2]	Hollister (1974), Gilroy Array#1, FF	0.67	EQ-I	0.14
Eq-2s		San Fernando (1971), Hollywood Storage, FF	1.00	EQ-II	0.23
Eq-3s		Imperial Valley (1940), Elcentro, FF	1.00	EQ-III	0.49
Eq-4s		Northridge (1994), Sylmar, NF	1.00	EQ-IV	0.71
IM-a	Long duration motions used in Rahman and Sritharan [9]	Morgan Hill (1984), Gilroy Array#6, NF	0.65	EQ-I	0.19
IM-b		Loma Prieta (1989), Saratoga Aloha Avenue, NF	0.64	EQ-II	0.32
IM-e		Kobe-Japan (1995), KJM, NF	0.94	EQ-III	0.56
NZ	Recordings from the past earthquakes	New Zealand (2011), HVSC, NF	0.40	EQ-II	0.58
Chile		Chile (2010), Angol, FF	1.00	EQ-III	0.49
Takatori	E-Defense Test [11]	Kobe-Japan (1995), Takatori, NF	0.60	EQ-IV	0.37

Note: NF = near-field motion; FF = far-filed motion

Table 2 – Test matrix and summary of results

Wall ID	Post-tensioning parameters		Shear resistance at 2% drift (kN)	Maximum response ratio ^a (drift, absolute acceleration, residual drift)	
	No., dia.(cm) of PT tendon	Initial PT stress (f_{pi} , MPa)		DBE	MCE
SRW1	4, 1.27	$0.64 f_{pu}$	151	Not applied	Not applied
SRW1m ^b		$0.30 f_{pu}$	104	2.91, 0.31, 0.18	2.79, 0.14, 0.1
SRW2	6, 1.27	$0.50 f_{pu}$	187	1.72, 0.64, 0.07	1.8, 0.42, 0.05
SRW3	6, 1.52	$0.63 f_{pu}$	297	0.83, 0.9, 0.01	0.88, 0.61, 0.01
SRW3m ^b	3, 1.52	$0.62 f_{pu}$	160	Not applied	1.03, 0.43, 0.15
SRW4	6, 1.52	$0.62 f_{pu}$	358	0.51, 0.63, 0.09	0.76, 0.34, 0.04
SRW4m ^b	3, 1.52	$0.51 f_{pu}$	174	Not applied	1.9, 0.17, 0.05

^a Maximum response to the allowable limit.

^b SRW1m, SRW3m, and SRW4m; after 50% loss in the initial PT force of SRW1, SRW3, and SRW4.

3. Participation of Different Damping Components

In addition to the inherent viscous damping, SRWs provide limited hysteresis damping due to concrete nonlinearity at wall toes and due to inelastic strains in PT tendons if they experience yielding. These walls also dissipate the energy imparted to them during an earthquake through impacts of the rocking of the wall on top of the footing. When subjected to a lateral load, a wall panel secured with unbonded post-tensioning rocks on top of the foundation, with a single gap opening and closing at its base. During contact between the wall panel and foundation, kinetic energy of relative motion is transformed into internal energy of deformation known as the strain energy by the contact force. A part of this internal energy is released, enabling the wall to bounce back while the rest of the energy is radiated back to the foundation. As a result, wall starts to rotate from one corner to the opposite corner with a smaller kinetic energy. The ratio of kinetic energy immediately after and immediately before an impact is called coefficient of restitution, r , and is used as a measure of the energy loss due to impacts as presented in Eq. (1).

$$r = \left[\frac{\dot{\theta}_{after}}{\dot{\theta}_{before}} \right]^2 \quad (1)$$

where $\dot{\theta}_{after}$ and $\dot{\theta}_{before}$ are angular velocities of the rocking wall after and before an impact, which quantifies the kinetic energy.

Presuming the angular momentum about the point of impending impact is conserved because no external force is applied to the system, Housner [12] showed that this ratio could be related to the geometry of the block, by the expression defined as Eq. (2):

$$r = \left[1 - \frac{mR^2}{I_o} (1 - \cos 2\alpha) \right]^2 \quad (2)$$

where I_o is the moment of inertia of the rocking wall about point O (see Fig. 1) and other parameters are shown in Fig. 1.

While rocking wall is subjected to an earthquake excitation, Eq. (2) is not valid, since the angular momentum is not conserved, but the energy loss could be estimated using the fundamental equation (i.e., Eq. (1)).

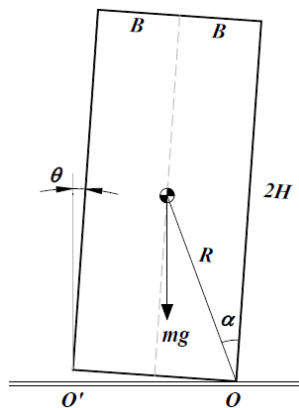


Fig. 1 – Housner rectangular rocking block [12]

Different energy dissipation components of test walls were evaluated during ground motions of DBE and MCE levels. Seismic input energy (E_I) dissipated through the inelastic action and inherent viscous damping of the test walls ($E_{hys} + E_{vis}$) were estimated using the experimental hysteresis loops. As presented in Fig. 2 for SRW2 during $0.8 \times Eq-4s$ – a DBE earthquake – the participation of energy dissipation due to impact (E_{imp}) was

noticeable. Estimating individual damping terms of the test walls during a series of DBE and MCE events confirmed that the impact energy loss was about 30%.

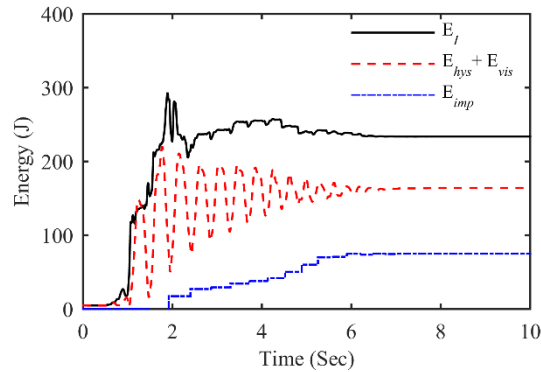


Fig. 2 – Participation of different damping components when SRW2 was subjected to 0.8×Eq-4s

4. Equivalent Viscous Damping Ratio

While energy dissipation of SRWs is conceived to be small, an appropriate estimate of the total damping encompassing all of the components was quantified using experimental data. Responses of SRWs to different intensities of Eq-4s and Takatori, representing EQ-III and EQ-IV hazard levels, were used to determine the equivalent viscous damping ratios of SRWs.

The equivalent viscous damping ratio of SRWs due to hysteretic action and inherent viscous damping ($\xi_{hys+vis}$) was estimated based on their measured hysteresis loop, using Eq. (3). This equation expresses the amount of damping corresponding to the area enclosed by each half-cycle of the hysteresis loop (A_h) defined by the maximum inertia force and displacement of F_m and Δ_m .

$$\xi_{area} = \frac{A_{half-loop}}{\pi F_m \Delta_m} \quad (3)$$

To represent the damping due to impact with a viscous damping ratio, the observed kinetic energy loss, as estimated from Eq. (1) during impacts was primarily reduced from instantaneous seismic energy transmitted to the system. This kinetic energy loss due to impacts was then accumulated for each input motion and equated to a continuous energy dissipation using a viscous damping ratio, ξ_{imp} .

Based on the experimental observations during a set of Takatori and Eq-4s motions, an average equivalent viscous damping ratio of 5.7% was established for SRWs with respect to the secant stiffness of the system defined at 2% design lateral drift. The results from test walls, excluding SRW3, subjected to the DBE and MCE earthquakes are shown in Fig. 3. According to this figure, the total damping includes 1.5% for the energy loss due to impacts and 4.2% due to concrete nonlinearity and the inherent material damping of the test units as they experience drifts between 1.4% and 2.6%. A higher average value of 7% damping due to the hysteretic action and inherent viscous damping was obtained for SRW3, which is believed to be due to the unprotected wall base experiencing relatively more damage.

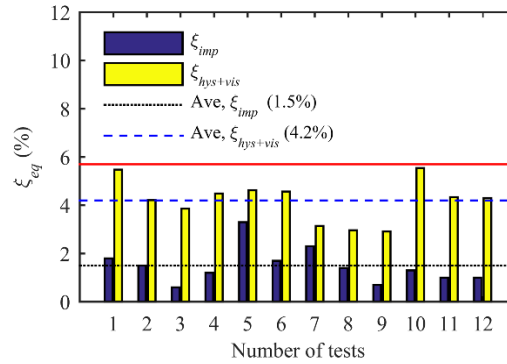


Fig. 3 – Equivalent viscous damping ratio of SRWs during different intensity levels of Takatori and Eq-4s

5. Dynamic Response

Recall that peak drifts of the test walls with larger base shear (e.g., SRW3 and SRW4) were below the allowable limits during DBE and MCE events; however, due to low amounts of damping, all SRWs were expected to undergo dynamic response for a longer duration. Therefore, this aspect was investigated.

Typical seismic responses of SRWs are shown in Fig. 4. In both cases, it is seen that the peak lateral drifts occurred during the input motion and the wall came to rest several seconds after the table acceleration (i.e., table feedback) subdued. Fig. 4a shows decay of the displacement response in SRW2 with an extended rocking period after experiencing large peaks during $0.8 \times \text{Eq-4s}$.

The negative rate of seismic energy (i.e., $E_I = - \int M_s \ddot{u}_g(t) du$) – the energy removed from the system – occurs when the ground acceleration (\ddot{u}_g) and the velocity response (du) of the system are in the same direction [13]. These favourable states mostly occur as period of the rocking wall gets larger compared to that of the excitation. This is shown in Fig. 4b, which compares the relative displacement response of SRW2 with the acceleration of the shake table during $1.4 \times \text{Takatori}$. The negative rate of seismic energy is revealed here to be the most probable cause that SRWs can control the extension of their dynamic response even after displacing to large drifts, although these walls are deemed to have limited damping capacity.

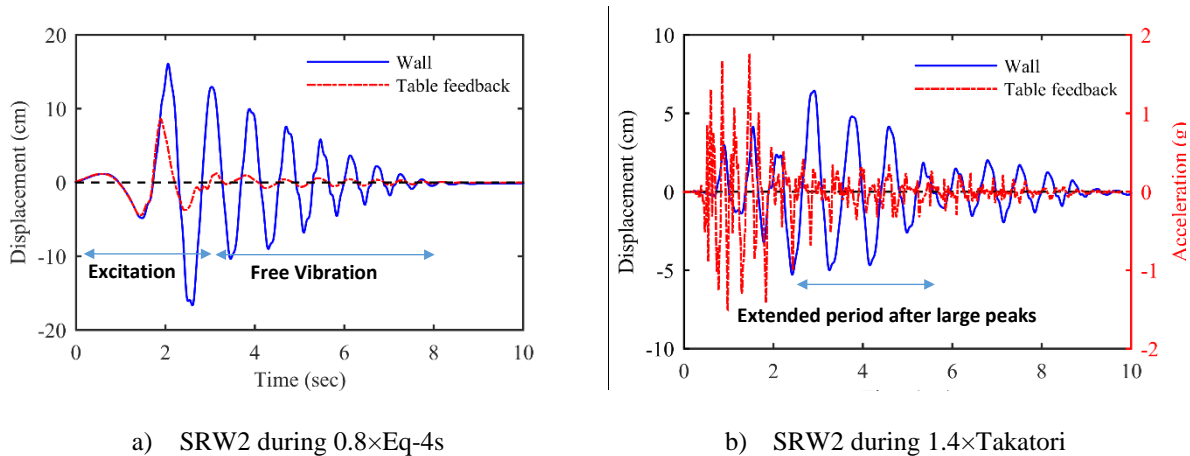


Fig. 4. The extended rocking period in SRWs following the peak displacement amplitude

6. Modelling SRW Damping

A lumped-plasticity SDOF model was developed in OpenSees [14] to capture the dynamic response of SRWs. Fig. 5 shows details of the model, including: (1) a rigid lumped mass representing the inertia effects; (2) an elastic beam column element modeling the precast concrete wall; and (3) a zero-length rotational spring to



capture the rocking interface with the assigned moment-rotation characteristics using a SelfCentering material model available in OpenSees.

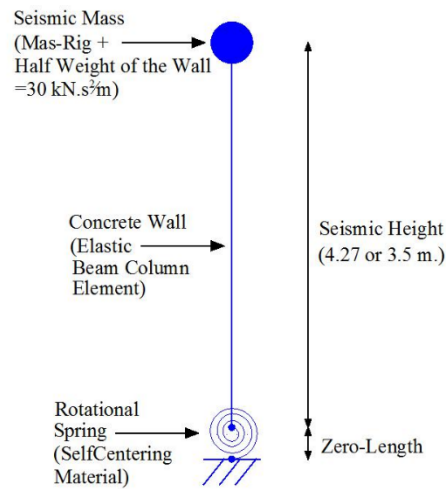


Fig. 5 – OpenSees model developed for a Single Rocking Wall

Results obtained from this analytical model and shake table testing were used to validate the accuracy of modeling different damping components and the overall response of SRWs. To represent the energy dissipation due to impacts, a 3% elastic viscous damping was included in the analysis using the tangent stiffness proportional Rayleigh damping in the model. Based on the recommendation of Priestly and Calvi [15], this was obtained by applying a multiplication factor of 2 to the secant stiffness based damping of 1.5%, as previously estimated.

Damping due to hysteretic action was also modeled by the flag-shape hysteresis response as captured with the SelfCentering material. Accordingly, a beta factor of 0.2 (for SRW2 with relatively no damage) or 0.3 (for SRW1m, SRW3, and SRW4 with higher damage to the concrete) was assigned to represent the energy dissipation of the system as a ratio of the yield force. Fig. 6, which presents the calculated equivalent damping ratios of the test walls for drift cycles between 1.4% and 2.6%, indicates an average damping of 3.8% associated with the inelastic response of SRW1m, SRW2, and SRW4, using the assumed hysteretic model; this compares closely with the average experimental value of 4.2% (see Fig. 3).

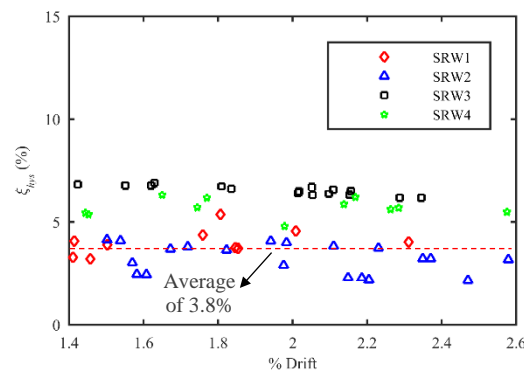


Fig. 6 – Equivalent damping ratio due to hysteretic action from the analytical model

Fig. 7 compares the experimental data with the calculated time-history lateral drift responses of SRWs, indicating that the assigned damping terms in the model satisfactorily emulate the shake table test results in terms of peak displacements and decay of response. Fig.7a also demonstrates that the model adequately captures



the accumulated damage, by showing response of SRW1m to a sequence of input motions with increasing intensity. Fig. 7b depicts the responses of SRWs to EQ-IV level records, which indicates that the peak drifts and overall responses are adequately captured even when subjected to the maximum considered earthquake motions.

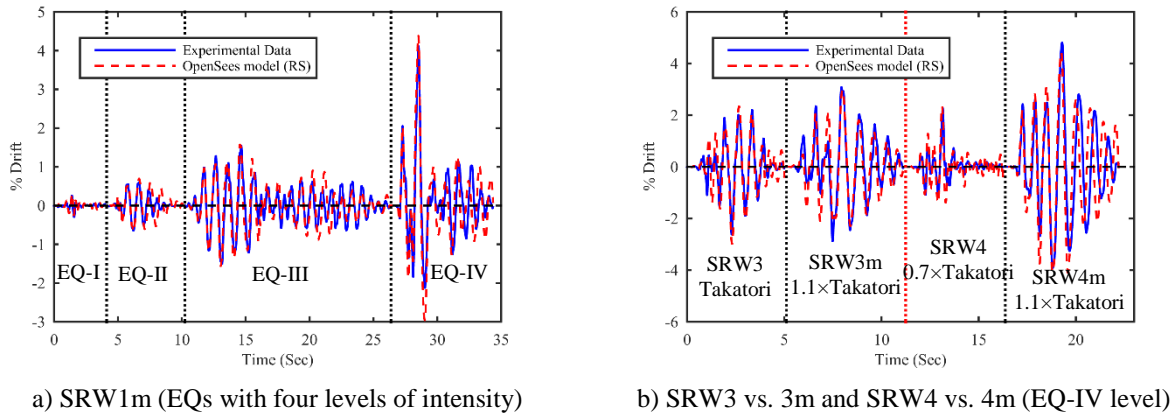


Fig. 7 Comparison between the experimental time-history lateral drift responses and the analytical results

7. Conclusions

Using shake table test data, this paper quantifies and compares different energy dissipation components of Single Rocking Walls with unbonded PT. The influence of damping due to impacts on dissipating the input seismic energy imparted to SRWs was evaluated using measured velocities. In addition to this damping component, it was shown that limited hysteretic action due to concrete nonlinearity at wall toes contributes to the energy dissipation in SRWs. The equivalent viscous damping ratio of SRWs due to their individual energy dissipating components was then evaluated. Accordingly, a 5.7% damping ratio was assigned to them, which comprised of 1.5% damping due to impacts and 4.2% damping due to hysteretic action and inherent viscous damping. It is demonstrated that these damping components can be accurately modelled by using a 3% tangent stiffness proportional elastic damping and a flag-shape hysteresis characteristic assigned to a single rotational spring modelling the rocking interface in SRWs. Comparison of the experimental and analytical results of different walls confirmed the accurate representation of damping in the SRW models. It was highlighted in this paper that the extended rocking period of SRWs after experiencing large rocking responses, favourably removed a part of the seismic energy. This helped to reduce duration of the rocking response of SRWs.

8. Acknowledgements

The study reported in this paper was based upon the NEES Rocking Wall project (<http://sri.cce.iastate.edu/NEES-Rocking-Wall/>) supported by the National Science Foundation under Grant No. CMMI-1041650 and Dr. Joy Pauschke served as the program director for this grant. Any opinions, findings, and conclusions or recommendations expressed in this material are those of the authors and do not necessarily reflect the views of the National Science Foundation. All shake table tests were conducted using the NEES shared facility at the University of Nevada, Reno (UNR). The test units were donated by Clark Pacific and MidState Precast through coordination by PCI West. Materials provided by Sumiden Wire, GTI, Hayes Industries and help provided by ironworker local 118 with post-tensioning of specimens are also gratefully acknowledged.



9. References

- [1] Kurama Y, Sause R, Pessiki S, Lu L (1999): Lateral load behavior and seismic design of unbonded post-tensioned precast concrete walls. *ACI Structural Journal*, **96**(4), 622–632.
- [2] Priestley MJN, Sritharan S, Conley JR, Pampanin S (1999): Preliminary results and conclusions from the PRESSS five-story precast concrete test building. *PCI Journal*, **44**(6), 42–67.
- [3] Restrepo J, Rahman A (2007) Seismic performance of self-centering structural walls incorporating energy dissipators. *Journal of Structural Engineering*, **133**(11), 1560–1570.
- [4] Sritharan S, Aaleti S, Henry R, Liu K, Tsai K (2015) Precast concrete wall with end columns (PreWEC) for earthquake resistant design. *Earthquake Engineering and Structural Dynamics*, **44**(12), 2075–2092.
- [5] Marriott D, Pampanin S, Bull D, Palermo A (2008) Dynamic testing of precast, post-tensioned rocking wall systems with alternative dissipating solutions. *Bulletin of the New Zealand Society for Earthquake Engineering*, **41**(2), 90–103.
- [6] Twigden, KM (2016) Dynamic response of unbonded post-tensioned concrete walls for seismic resilient structures, PhD Thesis. University of Auckland.
- [7] Seismology Committee (1999) Recommended lateral force requirements and commentary (Blue book). Structural Engineers Association of California (SEAOC), California, USA.
- [8] Aaleti S, Sritharan S (2009) A simplified analysis method for characterizing unbonded post-tensioned precast wall systems. *Engineering Structures*, **31**(12), 2966–2975.
- [9] Rahman M, Sritharan S (2006) An evaluation of force-based design vs. direct displacement-based design of jointed precast post-tensioned wall systems. *Earthquake Engineering and Engineering Vibration*, **5**(2), 285–296.
- [10] Nazari M, Sritharan S, Aaleti S (2014) Shake table testing of unbonded post-tensioned precast concrete walls. *Proceedings of the 10th National Conference in Earthquake Engineering*, Earthquake Engineering Research Institute, Anchorage, AK.
- [11] Tuna Z, Gavridou S, Wallace J (2012) 2010 E-defense four-story reinforced concrete and post-tensioned buildings—preliminary comparative study of experimental and analytical results. *Proceedings of the 15th World Conference on Earthquake Engineering*, Lisbon, Portugal.
- [12] Housner G (1963) The behavior of inverted pendulum structures during earthquakes. *Bulletin of the Seismological Society of America*, **53**(2), 403–417.
- [13] Dejon MJ (2012) Amplification of rocking due to horizontal ground motion. *Earthquake Spectra*, **28**(4), 1405–1421.
- [14] McKenna F, Fenves G, Scott M (2000) Open system for earthquake engineering simulation. University of California, Berkeley, CA.
- [15] Priestley M, Calvi GM, Kowalsky MJ (2007) Displacement-based seismic design of structures. *Building*, **23**(33), 1453–1460.